Light–Activated Tandem Catalysis Driven by Multicomponent Nanomaterials

8 AUTHORS, INCLUDING:

Elsayed Zahran
University of Miami
15 PUBLICATIONS **161** CITATIONS

Yao-Jen Chang
University of Kentucky
3 PUBLICATIONS **27** CITATIONS

Beth Guiton
University of Kentucky
25 PUBLICATIONS **837** CITATIONS

Light-Activated Tandem Catalysis Driven by Multicomponent Nanomaterials

Elsayed M. Zahran,[†] Nicholas M. Bedford,[‡,†] Michelle A. Nguyen,[†] Yao-Jen Chang,[§] Beth S. Guiton,[§,⊥] Rajesh R. Naik,[‡] Leonidas G. Bachas,*,[†] and Marc R. Knecht*,[†]

[†]Department of Chemistry, University of Miami, Coral Gables, Florida 33146, United States

[‡]Materials and Manufacturing Directorate, Air Force Research Laboratory, Wright-Patterson Air Force Base, Ohio 45433, United States

[§]Department of Chemistry, University of Kentucky, Lexington, Kentucky 40506, United States

[⊥]Materials Science and Technology Division, Oak Ridge National Laboratory, Oak Ridge, Tennessee 37831, United States

S *Supporting Information*

ABSTRACT: Transitioning energy-intensive and environmentally intensive processes toward sustainable conditions is necessary in light of the current global condition. To this end, photocatalytic processes represent new approaches for H_2 generation; however, their application toward tandem catalytic reactivity remains challenging. Here, we demonstrate that metal oxide materials decorated with noble metal nanoparticles advance visible light photocatalytic activity toward new reactions not typically driven by light. For this, Pd nanoparticles were deposited onto Cu_2O cubes to generate a composite structure. Once characterized, their hydrodehalogenation activity was studied via the reductive dechlorination of polychlorinated biphenyls. To this end, tandem catalytic reactivity was observed with H_2 generation via H_2O reduction at the Cu_2O surface, followed by dehalogenation at the Pd using the *in situ* generated H_2. Such results present methods to achieve sustainable catalytic technologies by advancing photocatalytic approaches toward new reaction systems.

Catalytic technologies must be redesigned for optimal reactivity under sustainable conditions with minimal to no energy input. Nanotechnology provides new avenues to achieve such sustainability goals without compromising the reactivity.[2] Furthermore, nanomaterial syntheses have recently matured to allow for the production of highly refined particles with control of the size, shape, and morphology of the structure;[3] however, the ability to design multicomponent nanosystems remains challenging. Such systems are likely to be highly important, especially for tandem catalytic reactions that require multiple catalysts interfaced into a single system.

Nano- and microscale metal oxides have been the focus of research due to their photoinduced electrical properties.[4] This phenomenon can be exploited for important photocatalytic reactions that drive redox-based chemical processes,[5] which arise from the semiconductor band gap; upon irradiation of the material with photons of appropriate energy, electron excitation from the valence to conduction band occurs, where the holes remain in the valence band. These electrons and holes then travel to the oxide surface to drive reduction and oxidation

reactions, respectively.[6] Given suitable band positions, this process can split water into H_2 and O_2.[7] As such, photocatalytic H_2 production is of enormous value, given the potential to generate significant energy sources using available resources and sunlight. Moreover, this sustainably produced H_2 could find other important uses in catalytic reactions such as hydrogenation and hydrodehalogenation, given the scale at which these reactions are performed. Decorating the metal oxide with noble metal nanocatalysts could result in a tandem catalytic system for reactions that are not traditionally driven by light. As such, this approach could transition unsustainable catalytic processes toward more sustainable, light-driven methods.

Here we describe the production of multicomponent tandem nanocatalysts that exploit light for multistep reactivity (Scheme 1). In this regard, Cu_2O cubes are generated, where addition of

Scheme 1. Fabrication and Activity of Cu_2O/Pd Tandem Catalysts for Light-Driven Hydrodehalogenation
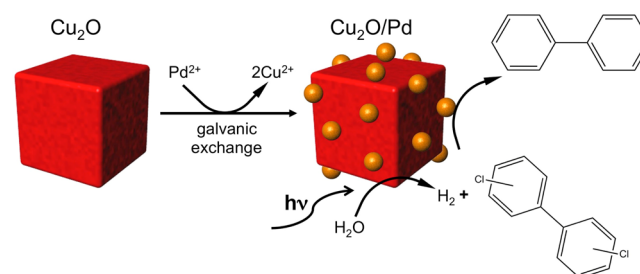
Pd^{2+} salts results in oxide surface decoration with Pd^0 nanoparticles via galvanic exchange. Once characterized, the materials were used for the hydrodehalogenation of polychlorinated biphenyls (PCBs), where quantitative reactivity to produce biphenyl was observed using just an aqueous solution and light. For this tandem catalytic system, the Cu_2O participates in H_2 production via photocatalysis that is subsequently activated on the Pd surface to drive hydrodehalogenation. These results are important for two key

reasons. First, they demonstrate a simple and aqueous-based method for the production of multicomponent tandem catalysts. Such catalytic systems can require surface immobilization to generate the appropriate structures,[8] thus increasing their synthetic complexity. Second, the materials are reactive using light as an energy source for reactions typically driven by an external H_2 source. As such, the adaptation of critically important sustainable approaches toward energy- and/or material-intensive processes is demonstrated.

The Pd-decorated Cu_2O (Cu_2O/Pd) materials were generated using a simple aqueous approach. To prepare the cubic Cu_2O component, a hydrothermal method was employed.[9] For this, 2.0 g of polyvinylpyrrolidone (PVP; 25000 g/mol) was added to 100 mL of a 0.035 mM aqueous Cu_2SO_4 solution. The mixture was stirred for 15 min, after which 100 mL of a solution of 0.07 mM sodium citrate and 0.12 mM Na_2CO_3 was added dropwise to hydrolyze the Cu_2SO_4 to $Cu(OH)_2$. Once prepared, the $Cu(OH)_2$ was then reduced to Cu_2O by the addition of 50 mL of 0.14 mM L,D-glucose. Following glucose addition, the system was heated at 80 °C for 2.0 h. The dark orange precipitate was filtered through a 200 nm track-etched polycarbonate membrane and dried at 60 °C overnight. The dried Cu_2O was then weighed and dispersed in EtOH, to which sufficient $Pd(O_2CCH_3)_2$ was added to reach 3 wt% Pd based upon the mass of Cu_2O. Due to the reduction potentials,[10] surface Cu^+ is oxidized to reduce the Pd^{2+} to Pd^0, resulting in the galvanostatic deposition of Pd nanoparticles onto the Cu_2O surface. The materials were left to react overnight, after which they were purified by filtration.

Once the multicomponent materials were fabricated, they were characterized using a variety of techniques. Initially, they were analyzed using powder X-ray diffraction (XRD) and X-ray photoelectron spectroscopy (XPS) (Figure 1). The XRD
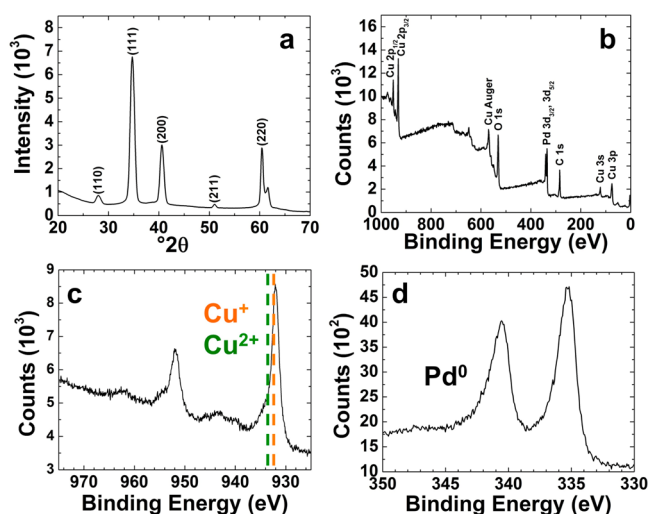
Figure 1. Cu_2O/Pd characterization: (a) X-ray diffraction pattern of the composite materials; (b) X-ray photoelectron spectrum of the structures. High-resolution XPS analysis of the materials at the (c) Cu and (d) Pd regions is also presented.

pattern (Figure 1a) was consistent with the cubic phase of Cu_2O, displaying reflections at 27.9, 35.1, 42.2, 50.1, and 61.4° 2θ, corresponding to the (110), (111), (200), (211), and (220) lattices in Cu_2O, respectively. Furthermore, no reflections arising from either CuO or Pd were observed. Such results suggest that Cu_2O is the dominant material present in the

sample. Additionally, the lack of Pd diffraction peaks suggests that this component is likely to be quite small in size and/or in significantly lower quantities as compared to the oxide. The XRD data are corroborated by the XPS spectrum of the composite materials (Figure 1b–d). The complete spectrum of the Cu_2O/Pd structures (Figure 1b) indicated that both Cu and Pd were present in the sample. High-resolution analysis of the Cu binding energy region (Figure 1c) demonstrated a peak at 932.2 eV for Cu $2p_{3/2}$, which is consistent with values for Cu^+.[11] XPS peak fitting (Supporting Information, Figure S1) indicated that the surface of the Cu component was comprised of 86.1% Cu^+, 12.8% Cu^{2+}, and 1.1% Cu^0. This was consistent with the XRD study indicating a negligible quantity of Cu^{2+} and Cu^0 impurities. Analysis of the Pd binding energy region (Figure 1d) demonstrated two peaks at 335 and 340.8 eV, corresponding to Pd $3d_{3/2}$ and $3d_{5/2}$, respectively.[12] These peaks were attributed to Pd^0, and no peaks associated with unreduced Pd^{2+} or PdO were evident.

Further characterization of the Cu_2O/Pd materials was conducted using both scanning and transmission electron microscopy (SEM and TEM, respectively). Figure 2a presents
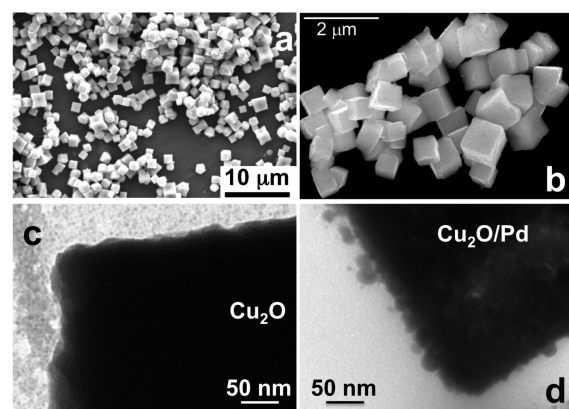
Figure 2. EM characterization: (a,b) SEM images and (c,d) TEM images of the Cu_2O cubes before (a,c) and after (b,d) Pd deposition.

the morphology of the bare Cu_2O materials. From this, well-defined cubic structures were generated with an edge length of 700 ± 120 nm, as determined from at least 100 particles. SEM analysis of the materials after Pd deposition is presented in Figure 2b. For these structures, the incorporation of Pd particles did not significantly alter the size of the materials (690 ± 110 nm). As anticipated, the Pd component on the faces of the cubes could not be observed using SEM, likely due to their small size. Energy-dispersive spectroscopy (EDS) analysis (Supporting Information, Figure S2) confirmed the Pd content of 3.0 wt%, consistent with the synthesis. Finally, TEM imaging of the Cu_2O and Cu_2O/Pd materials was also conducted. These images focus on the edge of the cubes to observe the difference in surface morphology arising from Pd incorporation. Figure 2c presents the TEM image of bare Cu_2O cubes, while Figure 2d displays Cu_2O/Pd structures. Here, Pd nanoparticles (16.1 ± 5.0 nm) are evident along the edge of the structure. Additional images are presented in the Supporting Information, Figure S3.

Due to the thickness of the Cu_2O, lattice-resolved imaging of the composite was not possible, especially along the cube faces. To confirm the location of the Cu and Pd regions of the Cu_2O/Pd structures, EDS mapping of the materials was conducted using annular dark-field scanning TEM (ADF-STEM)
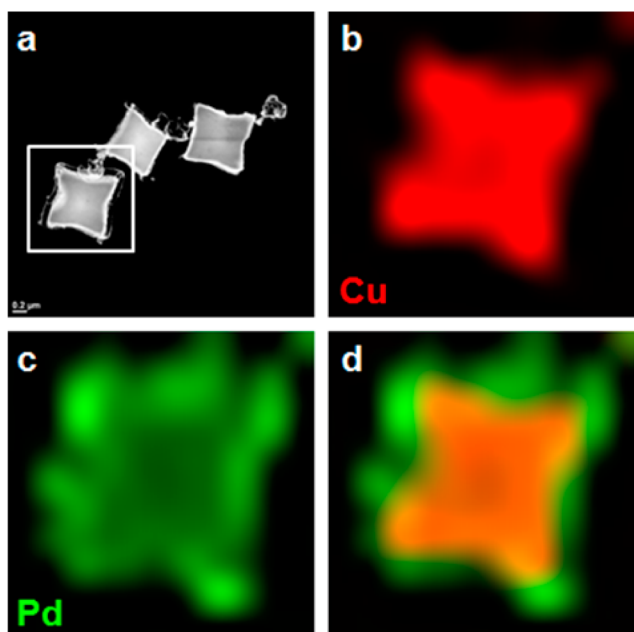
Figure 3. Compositional EDS mapping of the Cu_2O/Pd structures using STEM: (a) annular dark-field image of the materials; (b,c) the Cu and Pd maps, respectively; and (d) composite overlay of the Pd and Cu maps, demonstrating the Pd-decorated Cu_2O structure.

equipped with an EDS detector; Cu was detected at 8.04 keV and Pd at 2.84 keV. Figure 3 presents the elemental map and overlay for the composite structures. The images confirm that the Pd component was deposited along the surface of the Cu_2O cubes, forming the Cu_2O/Pd. This design is likely to enhance the catalytically reactive surface area due to the morphology at the interface between the two components. Indeed, based upon BET surface analysis, the area of the bare Cu_2O cubes was 0.99 m^2/g, which increased to 1.82 m^2/g after Pd nanoparticle deposition. Such an increase is important to efficiently expose the reactive materials for catalysis; however, this value is still somewhat low.

Once the structure of the Cu_2O/Pd materials was confirmed, their catalytic activity for light-driven hydrodehalogenation was processed. In this sense, a tandem catalytic reaction is anticipated (Scheme 1). First, H_2 generation should occur via H_2O reduction by the Cu_2O, driven by light. Next, this H_2 will be activated on the Pd, where hydrodehalogenation can occur. For this, the dechlorination of PCBs to generate biphenyl and Cl^- was examined (Figure 4 and Supporting Information, Tables S1 and S2). Such solution reactions are highly important for both organic synthesis and environmental decontamination.[13] Although metal oxides such as TiO_2 have been used for PCB breakdown,[14] this oxidative approach leads to the formation of hydroxylated PCBs that are more reactive with cell components,[15] as well as dioxins and furans that are significantly more toxic than the parent compounds.[15] Conversely, reductive dechlorination ultimately produces biphenyl that is less toxic than the parent PCB.[16] Such reductive methods typically require a separate H_2 source, which is introduced either via Fe^0 corrosion or through exogenous sources.[17] Both approaches are energy intensive and limited due to catalyst consumption; thus, new methods are required.

To demonstrate the tandem catalysis, reductive dechlorination of 3-chlorobiphenyl (PCB2) was examined using the Cu_2O/Pd structures (Figure 4a,b). For this reaction, 100 mg of
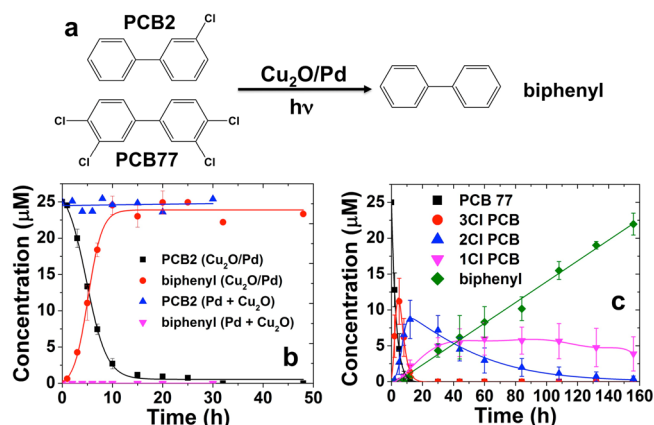

Figure 4. Tandem catalytic analysis for the light-driven dehalogenation reaction: (a) the mechanism, and reaction analysis as a function of time for (b) PCB2 and (c) PCB77.

the Cu_2O/Pd materials was added to 50 mL of a 25 mM PCB2 solution, resulting in a 2 mg/mL material concentration. The reaction was tightly sealed and then irradiated using a 450 W medium pressure mercury-vapor lamp in a light box. Aliquots were extracted at selected time points and quantitated using standard GC-MS methods to monitor reaction progress in triplicate.[17,18] Under these conditions, ~95% of the PCB2 was fully dechlorinated to biphenyl within 15 h, while quantitative product formation was observed at 30 h. In this system, no evidence of oxidative dechlorination was noted. As anticipated, when the same reaction was conducted in the dark, no dechlorination of PCB2 was observed.

To confirm that the reactivity arose from the tandem catalytic reductive hydrodehalogenation process, a set of controls was completed. First, when PCB2 was irradiated in the absence of Cu_2O/Pd, no dechlorination was evident after 48 h. Second, when the reaction was conducted with bare Cu_2O cubes (no Pd particles), again no dechlorination was observed. Third, in the standard tandem system, the PCB2 substrate was substituted with biphenyl to observe any potential breakdown of the final product. After 100 h of reaction, no change in the biphenyl concentration was noted. Fourth, when the Cu_2O/Pd reaction concentration was decreased by half, reactivity was retained; however, slower substrate conversion was observed (Supporting Information, Figure S4). Finally, when the reaction was performed using a physical mixture of Cu_2O cubes and separate Pd nanoparticles, no dechlorination was evident (Figure 4b). Note that the Pd nanoparticles were reactive for dechlorination using an exogenous H_2 source. Taken together, these results suggest that dechlorination driven by the Cu_2O/Pd materials follows a reductive pathway. For this, the Cu_2O facilitates H_2 generation via H_2O reduction, while the Pd controls PCB dechlorination using the *in situ* generated H_2. Note that EtOH was present in the system to increase PCB solubility, thus serving as a sacrificial reagent to prevent Cu_2O photocorrosion.

This unique architecture provides the Cu_2O/Pd materials with advantages over the individual components. For instance, photoinduced charge separation within the Cu_2O provides an electron for H_2 generation, which is then used to perform hydrodechlorination on the Pd. The close proximity of Cu_2O to Pd is advantageous to minimize diffusion effects that could limit or inhibit reactivity. Furthermore, as the Fermi level of Pd is lower than the conduction band (CB) of Cu_2O, photoexcited

electrons are shuttled from the CB of the oxide to the Fermi level of the metal.[17,19] Such charge transfer greatly decreases the likelihood of electron−hole recombination to enhance the photocatalytic activity, as shown previously for TiO_2/metal particle systems.[20] Moreover, the surface Pd could also facilitate the reduction of protons to form H_2 using the electron originating from the CB of the Cu_2O.[7a] As such, H_2 production could occur from both the Cu_2O and Pd surfaces. Taken together, the ensemble of the Pd particles on the Cu_2O cubes simultaneously provides localized catalytic sites for the hydrodehalogenation reaction in the vicinity of the photogenerated H_2.

To further investigate the reactivity of the Cu_2O/Pd materials, they were used for the dechlorination of 3,3′,4,4′-tetrachlorobiphenyl (PCB77). Identical reaction conditions were employed as compared to the PCB2 system; however, longer reaction times were monitored due to the greater number of chlorine groups. In this case, the reductive dechlorination pathway of PCB77 follows a stepwise removal of a single chlorine from the rings, where lower chlorinated derivatives can be measured during the course of the reaction. As shown in Figure 4c, complete removal of a single chlorine from PCB77 was achieved in 8 h to generate a PCB with three chlorine substituents. In this regard, a mixture of three-chlorine PCB congeners was observed that are combined to form the 3Cl PCB curve. As the photodriven reaction proceeded, a stepwise pattern representing the reductive dechlorination of PCB77 was noted, where biphenyl was the ultimate product. Nearly quantitative yields (90.5 ± 1.5%) of biphenyl were observed after 156 h; however, a small amount of 1Cl PCBs remained (9.5 ± 2.3%). As such, the materials are highly reactive for long-term dechlorination, as evidenced by their reactivity for the polychlorinated reagent.

In summary, we have demonstrated the generation of a multicomponent tandem nanocatalyst based upon Pd-decorated Cu_2O materials. These structures were fabricated using a facile electroless method, where the Pd particles are deposited on the surface of the Cu_2O cubes. This architecture provides advantages for light-activated tandem catalytic reactions that are dependent upon H_2 as a reagent. The Cu_2O/Pd materials demonstrated significant tandem catalytic functionality for the dechlorination of PCBs, which occurred via a reductive process, generating no toxic oxidation products. It is anticipated that this unique light-activated system could establish the foundation for the development of a new class of materials for sustainable reactivity that is dependent upon the use of H_2.

ASSOCIATED CONTENT

Ⓢ Supporting Information

Materials, methods, XPS fitting, TEM, EDS, and catalytic analysis. This material is available free of charge via the Internet at http://pubs.acs.org.

AUTHOR INFORMATION

Corresponding Authors
bachas@miami.edu
knecht@miami.edu

Notes
The authors declare no competing financial interest.

REFERENCES

(1) (a) Cole-Hamilton, D. J. *Science* **2003**, *299*, 1702. (b) Corma, A.; Garcia, H.; Xamena, F. X. L. I. *Chem. Rev.* **2010**, *110*, 4606.

(2) (a) Bhandari, R.; Coppage, R.; Knecht, M. R. *Catal. Sci. Technol.* **2012**, *2*, 256. (b) Li, Q.; Guo, B. D.; Yu, J. G.; Ran, J. R.; Zhang, B. H.; Yan, H. J.; Gong, J. R. *J. Am. Chem. Soc.* **2011**, *133*, 10878.

(3) (a) Gonzalez, E.; Arbiol, J.; Puntes, V. F. *Science* **2011**, *334*, 1377. (b) El-Sayed, M. A. *Acc. Chem. Res.* **2004**, *37*, 326.

(4) Guo, J.; Chen, X. *Solar Hydrogen Generation: Transition Metal Oxides in Water Photoelectrolysis*; McGraw-Hill: New York, 2012.

(5) (a) Walter, M. G.; Warren, E. L.; McKone, J. R.; Boettcher, S. W.; Mi, Q.; Santori, E. A.; Lewis, N. S. *Chem. Rev.* **2010**, *110*, 6446. (b) Gomes Silva, C.; Juarez, R.; Marino, T.; Molinari, R.; Garcia, H. *J. Am. Chem. Soc.* **2011**, *133*, 595.

(6) Fujishima, A.; Honda, K. *Nature* **1972**, *238*, 37.

(7) (a) Paracchino, A.; Laporte, V.; Sivula, K.; Gratzel, M.; Thimsen, E. *Nat. Mater.* **2011**, *10*, 456. (b) Chen, X. B.; Shen, S. H.; Guo, L. J.; Mao, S. S. *Chem. Rev.* **2010**, *110*, 6503.

(8) Yamada, Y.; Tsung, C. K.; Huang, W.; Huo, Z. Y.; Habas, S. E.; Soejima, T.; Aliaga, C. E.; Somorjai, G. A.; Yang, P. D. *Nat. Chem.* **2011**, *3*, 372.

(9) Sui, Y. M.; Fu, W. Y.; Yang, H. B.; Zeng, Y.; Zhang, Y. Y.; Zhao, Q.; Li, Y. E.; Zhou, X. M.; Leng, Y.; Li, M. H.; Zou, G. T. *Cryst. Growth Des.* **2010**, *10*, 99.

(10) Haynes, W. M. *CRC Handbook of Chemistry and Physics*, 93rd ed.; CRC Press: Boca Raton, FL, 2012.

(11) Wang, W. Z.; Wang, G. H.; Wang, X. S.; Zhan, Y. J.; Liu, Y. K.; Zheng, C. L. *Adv. Mater.* **2002**, *14*, 67.

(12) Jiang, C. L.; Ranjit, S.; Duan, Z. Y.; Zhong, Y. L.; Loh, K. P.; Zhang, C.; Liu, X. G. *Nanoscale* **2009**, *1*, 391.

(13) (a) Lewis, S. R.; Datta, S.; Gui, M. H.; Coker, E. L.; Huggins, F. E.; Daunert, S.; Bachas, L.; Bhattacharyya, D. *Proc. Natl. Acad. Sci. U.S.A.* **2011**, *108*, 8577. (b) Narayanam, J. M. R.; Tucker, J. W.; Stephenson, C. R. J. *J. Am. Chem. Soc.* **2009**, *131*, 8756.

(14) Nomiyama, K.; Tanizaki, T.; Ishibashi, H.; Arizono, K.; Shinohara, R. *Environ. Sci. Technol.* **2005**, *39*, 8762.

(15) Nomiyama, K.; Tanizaki, T.; Arizono, K.; Shinohara, R. *Chemosphere* **2007**, *66*, 1138.

(16) Li, T. Y.; Chen, Y. M.; Wan, P. Y.; Fan, M. H.; Yang, X. J. *J. Am. Chem. Soc.* **2010**, *132*, 2500.

(17) Zahran, E. M.; Bhattacharyya, D.; Bachas, L. G. *J. Mater. Chem.* **2011**, *21*, 10454.

(18) Zahran, E. M.; Bhattacharyya, D.; Bachas, L. G. *Chemosphere* **2013**, *91*, 165.

(19) Bruix, A.; Rodriguez, J. A.; Ramirez, P. J.; Senanayake, S. D.; Evans, J.; Park, J. B.; Stacchiola, D.; Liu, P.; Hrbek, J.; Illas, F. *J. Am. Chem. Soc.* **2012**, *134*, 8968.

(20) Liu, S. X.; Qu, Z. P.; Han, X. W.; Sun, C. L. *Catal. Today* **2004**, *93−5*, 877.